Energy Storage Materials 23 (2019) 741–748

Contents lists available at ScienceDirect

Energy Storage Materials

journal homepage: www.elsevier.com/locate/ensm

Hybrid Mg/Li-ion batteries enabled by Mg^{2+}/Li^{+} co-intercalation in VS_4 nanodendrites

Yanrong Wang [a], Caixing Wang [a], Xu Yi [a], Yi Hu [a], Lei Wang [a], Lianbo Ma [a], Guoyin Zhu [a], Tao Chen [a], Zhong Jin [a,b,*]

[a] Key Laboratory of Mesoscopic Chemistry of MOE, Jiangsu Key Laboratory of Advanced Organic Materials, School of Chemistry and Chemical Engineering, Nanjing University, Nanjing 210023, China

[b] Shenzhen Research Institute of Nanjing University, Shenzhen 518057, China

ARTICLE INFO

Keywords:
Hybrid Mg/Li-ion batteries
Cathodes
Mg^{2+}/Li^{+} co-intercalation
VS_4 nanodendrites

ABSTRACT

Hybrid Mg^{2+}/Li^{+} batteries (MLIBs) are very intriguing energy storage devices that combine the advantages of Li and Mg electrochemical redox processes. However, the battery performances of MLIBs in previous researches are usually restricted by the fact that only Li^{+} ions are participated in the reactions on the cathodes. We propose that this obstacle can be overcome by significantly improving the diffusion/transfer kinetics of highly-polarized divalent Mg^{2+} ions in the cathode material, so that both Mg^{2+} and Li^{+} can be intercalated into the cathode material. Herein, we demonstrate that the electrochemical energy storage capability of MLIBs can be greatly improved by employing vanadium tetrasulfide (VS_4) nanodendrites as cathode material. Benefited from the special one-dimensional atomic-chain structure, the VS_4 nanodendrites are capable for the simultaneous reversible insertion/extraction of both Mg^{2+} and Li^{+} ions with fast diffusion kinetics, high capacity and long cycling stability. The MLIBs assembled with VS_4 nanodendrites cathodes exhibit a high reversible capacity of ~300 mAh g^{-1} at 500 mA g^{-1}, and a high cycle stability with the capacity maintained at 110 mAh g^{-1} after 1500 cycles at 1000 mA g^{-1}.

1. Introduction

Rechargeable lithium ion batteries (LIBs) play a significant role among existing portable energy storage technologies. However, LIBs are confronted with relatively low capacity, limited cycling life and safety issues [1]. Rechargeable magnesium ion batteries (MIBs) are receiving growing attention since the pioneering work of Aurbach et al., in 2000 [2,3], due to the potential advantages of high theoretical volumetric capacity (3833 mAh cm^{-3}), raw material abundance, and good safety originated from the dendrite-free deposition of metal Mg during charging/discharge processes [4–6]. These advantages have made MIBs a promising candidate of electrochemical energy systems. However, the insertion/extraction of divalent Mg^{2+} ions is more difficult than monovalent alkali cations (such as Li^{+} and Na^{+}). The strong Coulombic interaction between Mg^{2+} and host material lattices induces sluggish solid-state diffusion kinetics of Mg^{2+} ions within cathode materials [7]. It could lead to large polarization during charge/discharge, resulting in rapid capacity decay of cathode materials. To date, a variety of cathode materials have been proposed for MIBs, including Chevrel phase compounds [2], transition metal chalcogenides [4,8,9], metal oxides [10–12], and sulfur [13], etc. But most of these cathode materials still couldn't offer adequate capacity and cycling life for practical application. Therefore, the search of suitable cathode materials that can reversibly intercalate Mg^{2+} ions with high energy density is intrinsically challenging and essential.

An alternative solution to solve this problem is to construct hybrid Mg/Li-ion batteries (MLIBs) that combines the dendrite-free Mg anodes, the high-capacity cathodes for LIBs, and the dual-salt electrolyte containing both Mg^{2+} and Li^{+} ions [14–17]. In recent years, great efforts have been made on the research of MLIBs [18–23]. However, most of existing MLIBs have either a limited discharge capacity or a narrow electrochemical window. In the previous designs, normally only Li^{+} ions can participate in the reactions of cathode materials, therefore so far the battery performances of MLIBs are still restricted. It is highly desirable to develop advanced cathode materials that can efficiently accommodate both Mg^{2+} and Li^{+} ions.

* Corresponding author. Key Laboratory of Mesoscopic Chemistry of MOE, Jiangsu Key Laboratory of Advanced Organic Materials, School of Chemistry and Chemical Engineering, Nanjing University, Nanjing 210023, China.
E-mail address: zhongjin@nju.edu.cn (Z. Jin).

https://doi.org/10.1016/j.ensm.2019.06.001
Received 3 March 2019; Received in revised form 31 May 2019; Accepted 1 June 2019
Available online 6 June 2019

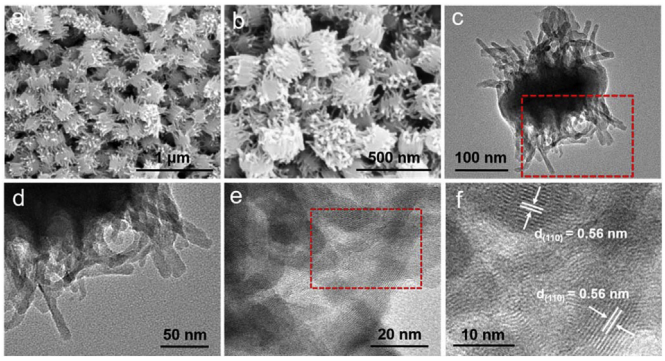

Fig. 1. (a, b) SEM images, (c–e) TEM images, (f) HRTEM image of as-prepared VS_4 nanodendrites.

Herein, we report that the energy storage performances of MLIBs can be significantly boosted by employing vanadium tetrasulfide (VS_4) nanodendrites as cathode material that can efficiently intercalate both Mg^{2+} and Li^+ ions. VS_4 is a 1D linear-chain compound, which composed of V^{4+} ions coordinated to sulfur dimers (S_2^{2-}) extending along the *c* axis [24]. The interval distance between the atomic chains is 5.83 Å, which is adequate for Mg^{2+} storage. The neighboring atomic chains of VS_4 are only interacted by weak van der Waals forces, which is favorable for ion transfer kinetics. Moreover, VS_4 has a narrow band gap of ~1.0 eV and shows relatively high conductivity [25]. Previous researches show that VS_4 has good Li^+ and Na^+ storage properties [26–29]. Recently, our group has confirmed that VS_4 cathode can also reversibly intercalate Mg^{2+} ions, exhibiting high capacity, exceptional rate performance and long cycling life in MIBs [30]. Here in this work, by combining metal Mg anodes, highly-branched VS_4 nanodendrites cathodes and a dual-salt electrolyte (phenylmagnesium chloride-$AlCl_3$/LiCl in tetrahydrofuran (THF) solution, termed as APC-LiCl electrolyte), high-performance MLIBs that can simultaneously realize the reversible electrochemical storage of both Mg^{2+} and Li^+ ions are successfully fabricated. Benefited from the co-intercalation of Mg^{2+} and Li^+ ions with fast kinetics and high reversibility in VS_4 nanodendrites, the specific capacity, rate capability and cycling stability of MLIBs are greatly improved.

2. Results and discussion

Through a modified solution-phase approach, highly-branched VS_4 nanodendrites consisted of numerous one-dimensional VS_4 nanorods were prepared [30]. The morphological characterizations of as-prepared VS_4 nanodendrites are shown in Fig. 1. The VS_4 nanodendrites have a uniform morphology assembled by nanorods with the diameter of ~10 nm and length of ~80 nm, which is conductive to electron transfer and Mg^{2+} diffusion (Fig. 1a–d). The high-resolution TEM (HRTEM) images (Fig. 1e and f) show a lattice plane spacing of 0.56 nm, consistent with the (110) planes of monoclinic phase VS_4.

X-ray powder diffraction (XRD) patterns confirmed the good crystallinity and high purity of as-obtained VS_4 nanodendrites (Fig. 2a), and all characteristic peaks are in good agreement with monoclinic phase VS_4. X-ray photoelectron spectroscopy (XPS) analysis was used to further investigate the chemical states of V and S elements (Fig. 2b and c). The peaks at 514.1 and 521.7 eV are assigned to V $2p_{3/2}$ and V $2p_{1/2}$ bands (Fig. 2b), which are the characteristic features of V^{4+}. The relatively weaker peaks at 516.8 and 524.3 eV were ascribed to V $2p_{3/2}$ and V $2p_{1/2}$ bands for V^{5+}, which could be derived from the slight oxidization on the surface upon exposure to air [10,31], indicating the content of V^{4+} is much higher than that of V^{5+}. The peaks at 162.9 and 164.0 eV were ascribed to S $2p_{3/2}$ and S $2p_{1/2}$ bands (Fig. 2c), respectively, indicating the presence of S_2^{2-} dimers. Bright-field scanning TEM (BF-STEM) and corresponding elemental mapping images (Fig. 2d–f) clearly show that the V and S atoms are homogeneously distributed in VS_4 nanodendrites. The survey XPS spectrum and energy dispersive X-ray spectroscopy (EDX) elemental analysis of VS_4 nanodendrites are shown in Fig. S1, indicating the coexistence of V and S atoms with an atomic percentage ratio right around 1:4. Fig. S2 shows the specific surface area of VS_4 nanodendrites is 48.9 $m^2 g^{-1}$.

To investigate the effects of Mg^{2+} and Li^+ intercalation, MIBs are fabricated by using APC electrolyte (THF solution of 0.4 M APC) and MILBs are fabricated by using APC-LiCl dual-salt electrolyte (THF solution of 0.4 M APC and 0.4 M LiCl), respectively, as detailed in the Experimental Section of Supporting Information. Both APC electrolyte and APC-LiCl dual-salt electrolyte are stable in the potential range between 0.2 and 2.2 V *vs.* Mg^{2+}/Mg [6,32–35]. Moreover, previous works have reported that different from Li^+, Mg^{2+} can't diffuse through the blocking layer formed by the reduced products on metallic Mg electrode [36,37]. The electrochemical performances of VS_4 nanodendrites as cathode material in MIBs and MLIBs were systematically measured and compared. The CV curves of VS_4 nanodendrites at the 1st, 2nd, and 5th cycles in MIBs and MLIBs are shown in Fig. 3a and b. The open circuit potential (OCV) for both MLIBs and MIBs are about 1.5 V. The reduction peak appears at ~0.80 V in the 1st cycle of MLIBs (Fig. 3a), and the relatively strong polarization in the 1st discharge process compared to the subsequent cycles is probably caused by the thin oxide layer on the surface of Mg anode [38]. Both MIB and MLIB show relatively lower discharge potential in the first cycle compared with the following cycles in Fig. 3c and d, which is also consistent with the CV curves in Fig. 3a and b. A reduction peak at ~1.17 V and an oxidation peak at ~1.30 V *vs.*

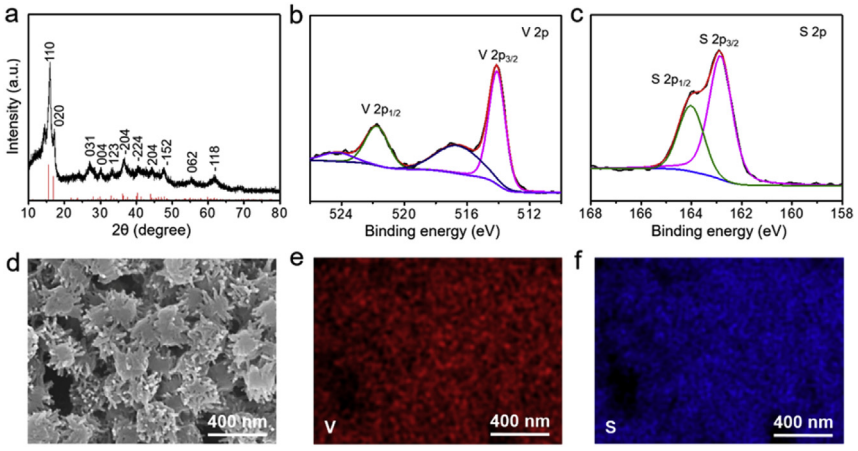

Fig. 2. (a) XRD pattern, (b, c) XPS spectra at (b) V 2p and (c) S 2p regions, (d) BF-STEM image and corresponding elemental mappings of (e) V and (f) S elements of VS_4 nanodendrites.

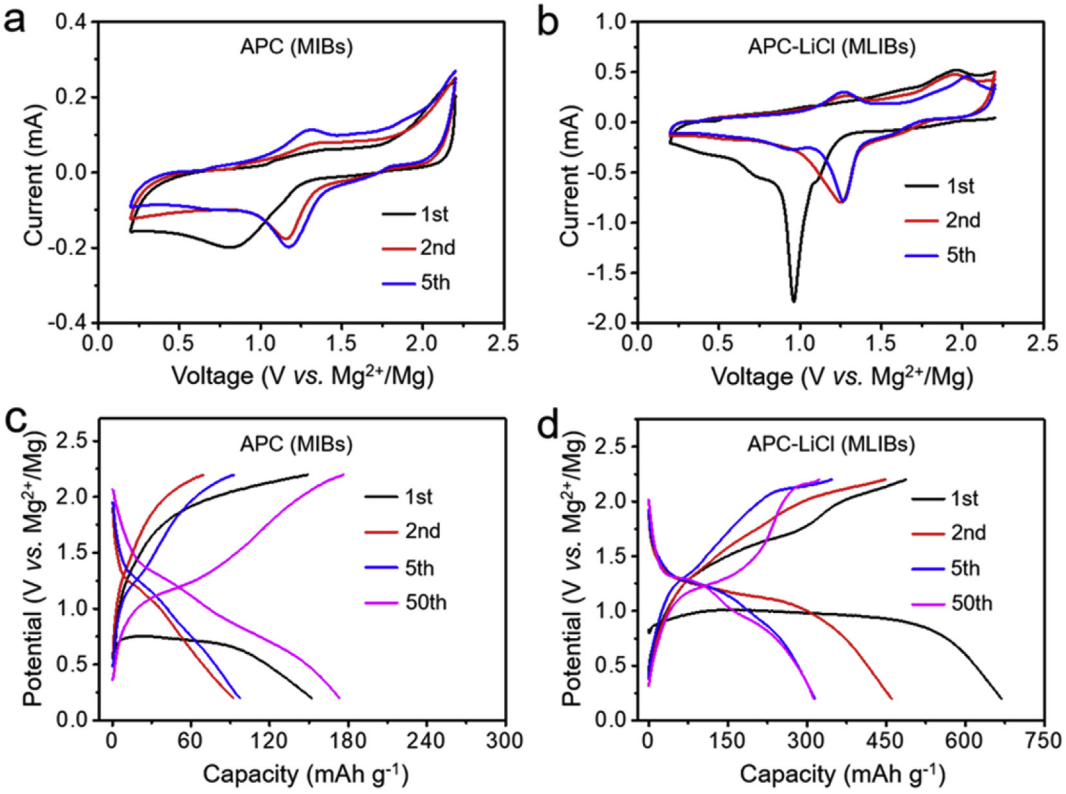

Fig. 3. CV curves of VS_4 nanodendrites in (a) MIBs (with APC electrolyte) and (b) MLIBs (with APC-LiCl electrolyte) cycling at a scanning rate of 0.2 mV s^{-1} in a potential range between 0.2 and 2.2 V *vs.* Mg^{2+}/Mg, respectively. Discharge-charge curves of VS_4 nanodendrites in (c) MIBs and (d) MLIBs at a current density of 500 mA g^{-1} after different cycles, respectively.

Mg^{2+}/Mg during the 2nd and 5th cycles are derived from the Mg^{2+} insertion/extraction into/from VS_4, respectively. In contrast, the reduction peaks of MLIBs in the 1st cycle appear at ~0.96 and 0.73 V, which are caused by the insertion of Li^+ and Mg^{2+} ions, respectively (Fig. 3b). Similar to MIBs, the polarization also occurs in the 1st discharge process. The insignificant broad oxidation peak at ~1.26 V is ascribed to the extraction of Mg^{2+} ions, and another oxidation peak at ~1.96 V is attributed to the extraction of Li^+ ions. During the 2nd cycle of MLIBs, a reduction peak at ~1.25 V and an oxidation peak at ~1.27 V are shown, resulting from the insertion of Mg^{2+} ions into VS_4 and extraction from VS_4, respectively. The broad reduction peak at ~1.56 V and broad oxidation peak at ~1.95 V are assigned to the Li^+ ion insertion into VS_4 and extraction from VS_4, respectively [29,39]. The CV curve in the 5th cycle is similar to that of the 2nd cycle, implying good reversibility of ions insertion/extraction in VS_4. Moreover, the peak intensities in the CV curves of MLIBs are greatly increased compared with those of MIBs, indicating the co-intercalation of Mg^{2+} and Li^+ ions in MLIBs, which is further confirmed by inductively-coupled plasma optical emission spectroscopy (ICP-OES) analysis (Table S1). It reveals that the contents of Mg^{2+} ions stored in VS_4 electrode during the discharge-charge processes are much higher than those of Li^+ ions. Moreover, ICP-OES (Table S1) and EDX data (Fig. S3) confirm that there are still a part of Mg^{2+} and Li^+ ions are remained in VS_4 lattices without extraction after charging to 2.2 V *vs.* Mg^{2+}/Mg.

Fig. 3c and d show the discharge-charge curves of VS_4 nanodendrites in MIBs and MLIBs at 500 mA g^{-1} during the 1st, 2nd, 5th and 50th cycles, respectively. The MLIBs based on VS_4 nanodendrites display similar discharge and charge potential platforms compared to the MIBs. However, the initial and subsequent discharge capacities of MLIBs are much higher than those of MIBs. At the 50th cycle, the discharge capacities of both MIBs and MLIBs display almost no drop compared to those at the 5th cycle, indicating the good cycling performances. For comparison, the discharge-charge curves of VS_4 nanodendrites in LIBs based on VS_4 nanodendrites cathodes and Li metal anodes at 500 mA g^{-1} are also shown in Fig. S4a. Considering that the redox potential of Mg^{2+}/Mg is 0.67 V higher than that of Li^+/Li, the potential window of LIBs was set between 1.0 and 3.0 V *vs.* Li^+/Li [19]. The LIBs show a flat discharge potential platform around 1.8–2.0 V *vs.* Li^+/Li and a high initial discharge capacity, but the discharge capacity rapidly drops to 31 mAh g^{-1} after 50 cycles and then 22 mAh g^{-1} after 100 cycles (Fig. S4b). This indicates that the capacity contribution of Mg^{2+} storage is much greater than Li^+ storage in MLIBs, which is consistent with the ICP-OES results (Table S1).

The high cycle stability of VS_4 in MIBs and MLIBs at 500 mA g^{-1} are shown in Fig. 4a. The discharge and charge capacities of MIBs in the first cycle are 152 and 85 mAh g^{-1}, respectively, with an initial Coulombic efficiency of ~56%. The discharge capability increases to 190 mAh g^{-1} after 200 cycles, with a Coulombic efficiency of nearly 100%. In contrast, the discharge and charge capacities of MLIBs in the first cycle are 668 and 487 mAh g^{-1}, respectively, corresponding to an initial Coulombic efficiency of 73%. The amount of Li^+ (64 μmol) is excess compared to the amount of VS_4 (12.8–17.3 μmol). The discharge capability maintains at 270 mAh g^{-1} after 200 cycles with a Coulombic efficiency close to 100%. These results indicate that with the help of Li^+ co-intercalation, the VS_4 nanodendrites as cathode material become more favorable for Mg^{2+} intercalation. The long-term cycling stability of VS_4 nanodendrites in MLIBs were further studied at a high current density of 1000 mA g^{-1} (Fig. 4b). The discharge capacity maintains at 150 mAh g^{-1} after 500 cycles, corresponding to a capacity retention of 71% compared to the 5th cycle. After 1500 cycles, a reversible capacity of 110 mA h g^{-1} was still retained, indicating an impressive stable cycling performance. The Coulombic efficiency keeps at nearly 100% due to the negligible charge trapping in the cathode, as well as the highly reversible and dendrite-free deposition of metal Mg.

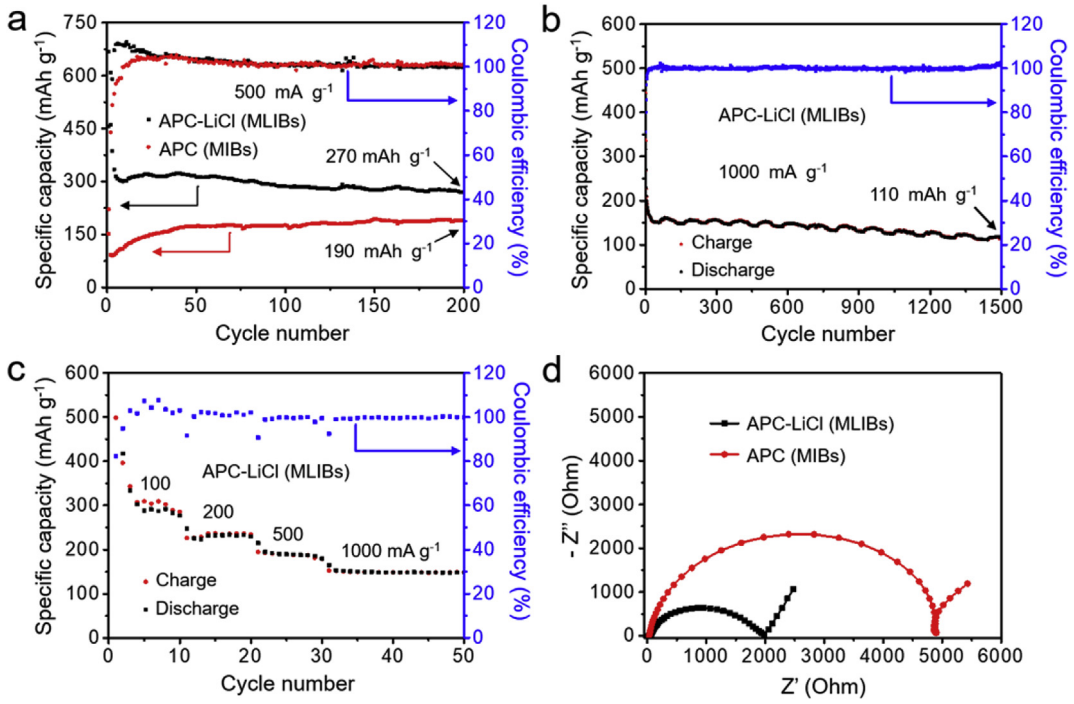

Fig. 4. Electrochemical performance comparison of VS_4 nanodendrites in MIBs (with APC electrolyte) and MLIBs (with APC-LiCl electrolyte): (a) Cycling performances of VS_4 nanodendrites in MIBs and MLIBs at a current density of 500 mA g^{-1}. (b) Long-term cycling test of VS_4 nanodendrites in MLIBs at 1000 mA g^{-1} for 1500 cycles. (c) Rate performance of VS_4 nanodendrites in MLIBs at the current densities ranged from 100 to 1000 mA g^{-1}. (d) EIS curves of VS_4 nanodendrites in MLIBs and MIBs.

Fig. 4c shows the rate capability of VS_4 nanodendrites in MLIBs cycling under various current densities. The discharge capacities are 288, 232, 189, and 150 mAh g^{-1} at 100, 200, 500, and 1000 mA g^{-1}, respectively. The discharge capacity still maintains at 245 mAh g^{-1} after 55 cycles when the current density returned back to 100 mA g^{-1}. The electrochemical impedance spectra (EIS) of VS_4 nanodendrites in MIBs and MLIBs are compared in Fig. 4d. The depressed semicircle in the high-frequency region can be ascribed to the charge transfer on the electrode/electrolyte interface, and the inclined line in the low-frequency can be attributed to the Warburg resistance, reflecting the ion diffusion resistance within the electrode, respectively. The charge transfer resistance of MLIBs is much lower than that of MIBs, confirming that the presence of Li^+ ions is beneficial to facilitate charge transfer kinetics, thus beneficial to the capacity and rate performance.

To investigate the ion storage mechanism of VS_4 in MLIBs, *ex-situ* XPS, *ex-situ* XRD, *ex-situ* Raman spectroscopy and *ex-situ* HRTEM were performed. As displayed in Fig. 5a–c, a series of *ex-situ* XPS spectra (V 2p, S 2p, Mg 2p and Li 1s energy levels) were collected from pristine, discharged and charged VS_4 cathodes, respectively. For the pristine VS_4 cathode, two dominating peaks at 514.0 eV and 521.7 eV are assigned to V $2p_{3/2}$ and V $2p_{1/2}$ bands of V^{4+}, and two relatively weaker peaks at 516.7 eV and 524.3 eV are attributed to V $2p_{3/2}$ and V $2p_{1/2}$ bands of V^{5+}, which are consistent with Fig. 2b. After discharged to 0.2 V, the intensities of the peaks at 516.4 eV and 523.7 eV are significantly increased, indicating the partial oxidation of V^{4+} to V^{5+}. According to the XPS results (Table S2), the atomic ratio of V^{4+}:V^{5+} after the 1st discharge step is calculated to be approximately 20:80. When fully charged to 2.2 V, the atomic ratio of V^{4+}:V^{5+} measured form the V 2p XPS spectrum is increased to about 30:70. In Fig. 5b, the S2p XPS spectrum of pristine VS_4 cathode shows two energy bands (162.9 and 164.1 eV) related to the S $2p_{3/2}$ and S $2p_{1/2}$ bands of S_2^{2-}, respectively. After discharged to 0.2 V, six new peaks are emerged. The two peaks at 162.2 and 163.2 eV are assigned to S $2p_{3/2}$ and S $2p_{1/2}$ bands of S^{2-}, respectively, confirming the partial reduction of S_2^{2-} to S^{2-} by the insertion of Mg^{2+} and Li^+ ions. The other four peaks at 160.7, 161.9, 159.7 and 160.8 eV could be assigned to MgS and Li_2S, respectively [40–43]. The atomic ratio of S_2^{2-} and S^{2-} species acquired from the XPS results (Table S2) is approximately 43:57. Another two peaks at 168.2 and 169.4 eV are derived from SO_x, which may be generated from the decomposition of THF solvent [6]. After charged to 2.2 V, the atomic ratio of S_2^{2-} (two peaks at 162.8 and 164.1 eV) and S^{2-} (two peaks at 162.4 and 163.6 eV) species is increased to 69:31. The atomic content of S^{2-} is decreased but still exists, which means the product has not fully converted to pristine VS_4 after charging. The XPS band intensities of Mg 2p and Li 1s after the 1st discharge process is stronger than those after the 1st charge process (Fig. 5c), confirming the reversible insertion/extraction of Mg^{2+} and Li^+ into/from VS_4. Clearly, some Mg^{2+} and Li^+ ions are remained in VS_4 lattices during the discharge/charge processes. Moreover, the intensity of Mg 2p band is much stronger than Li 1s band, consistent with the ICP-OES (Table S1) and EDX results (Fig. S3), indicating that Mg^{2+} storage play a leading role in the capacity contribution of MLIBs.

The *ex-situ* XRD analysis of VS_4 cathode at different discharge and charge states (from state *1* to state *5* in Fig. 5d) during the 1st cycle was also carried out (Fig. 5e). Two main peaks ascribed to the (110) and (020) planes were shown in pristine VS_4 electrode (state *1*). The peak locations didn't shift but the peak intensities were greatly changed during the discharge/charge processes (Fig. 5e). The intensities of the above two main peaks obviously decreased during the discharge process (from state *1* to state *3*), resulting from the insertion of Mg^{2+} and Li^+ ions into VS_4 lattices. The main peak intensities increased again due to the partial extraction of Mg^{2+} and Li^+ ions during the following charge process (from state *3* to state *5*).

Fig. 5f shows the *ex-situ* Raman spectra of VS_4 nanodendrites electrode at different discharge-charge states. For the pristine VS_4 electrode (state *1* in Fig. 5f), the modes at 191 and 217 cm^{-1} are originated from V–S bond stretching. The mode at 268 cm^{-1} is attributed to V–S bond bending. The mode at 346 cm^{-1} is originated from the breathing of V_2S_4-cages. Other modes at 288, 542 and 556 cm^{-1} are identified as S–S bond stretching/twisting [44,45]. During the discharge/charge processes, the above peaks appear almost no shift and no new peak appears, but there is

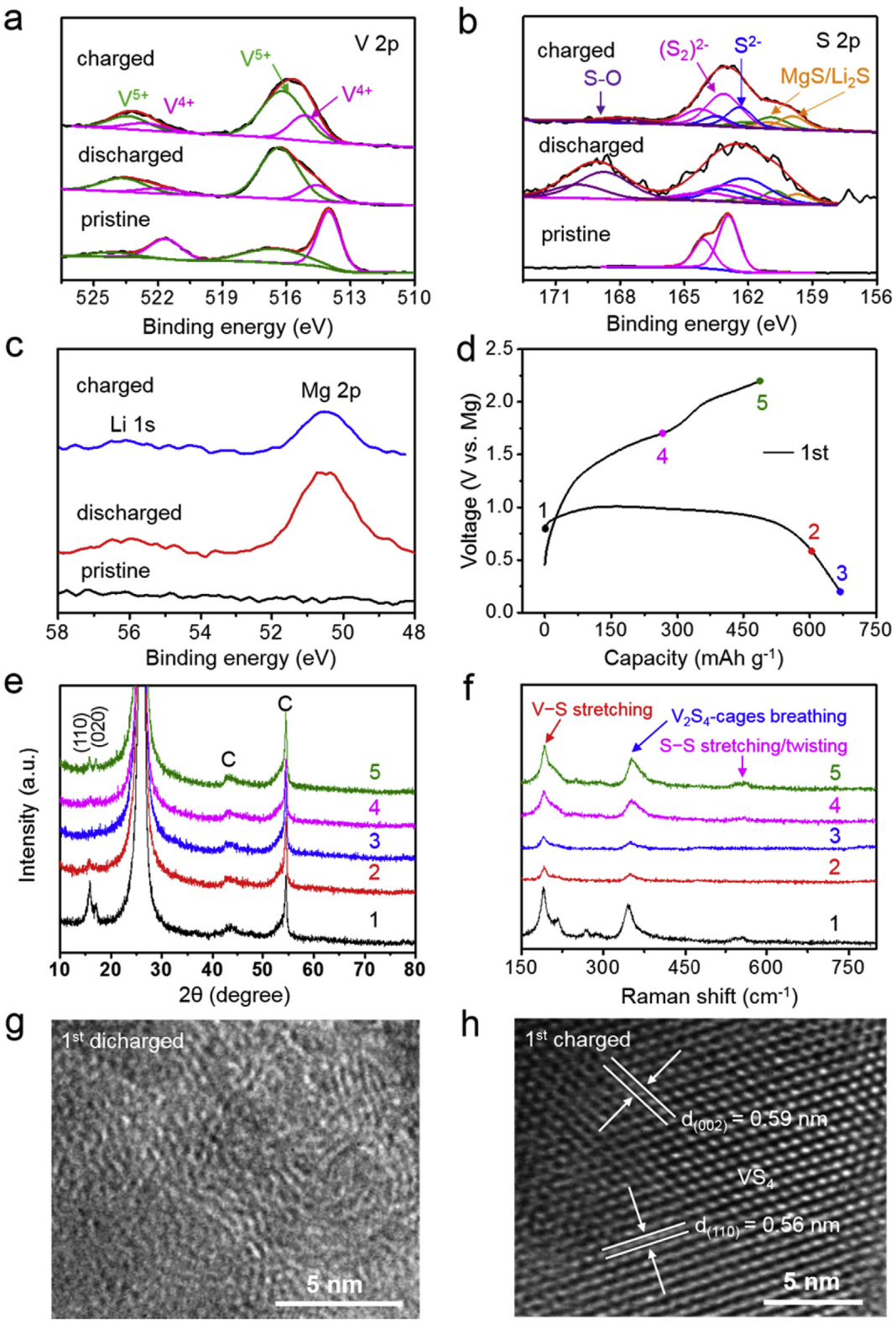

Fig. 5. (a–c) *Ex-situ* XPS spectra at the (a) V 2p, (b) S 2p, (c) Mg 2p and Li 1s regions of VS_4 nanodendrites cathode in MLIBs at different states: pristine, after the initial discharge step and after the initial charge step, respectively. (d) Discharge-charge profile during the initial cycle at 500 mA g^{-1}. The points labeled with *1–5* indicate the different discharge-charge states for the collection of XRD patterns in (e) and also Raman spectra in (f). (e) *Ex-situ* XRD patterns and (f) *Ex-situ* Raman spectra of VS_4 nanodendrites collected at various discharge-charge states. The peaks labeled by "C" are originated from the carbon paper served as the current collector. (g, h) HRTEM images of VS_4 nanodendrites cathode in MLIBs (g) after the 1st discharge step and (h) after the 1st charge steps.

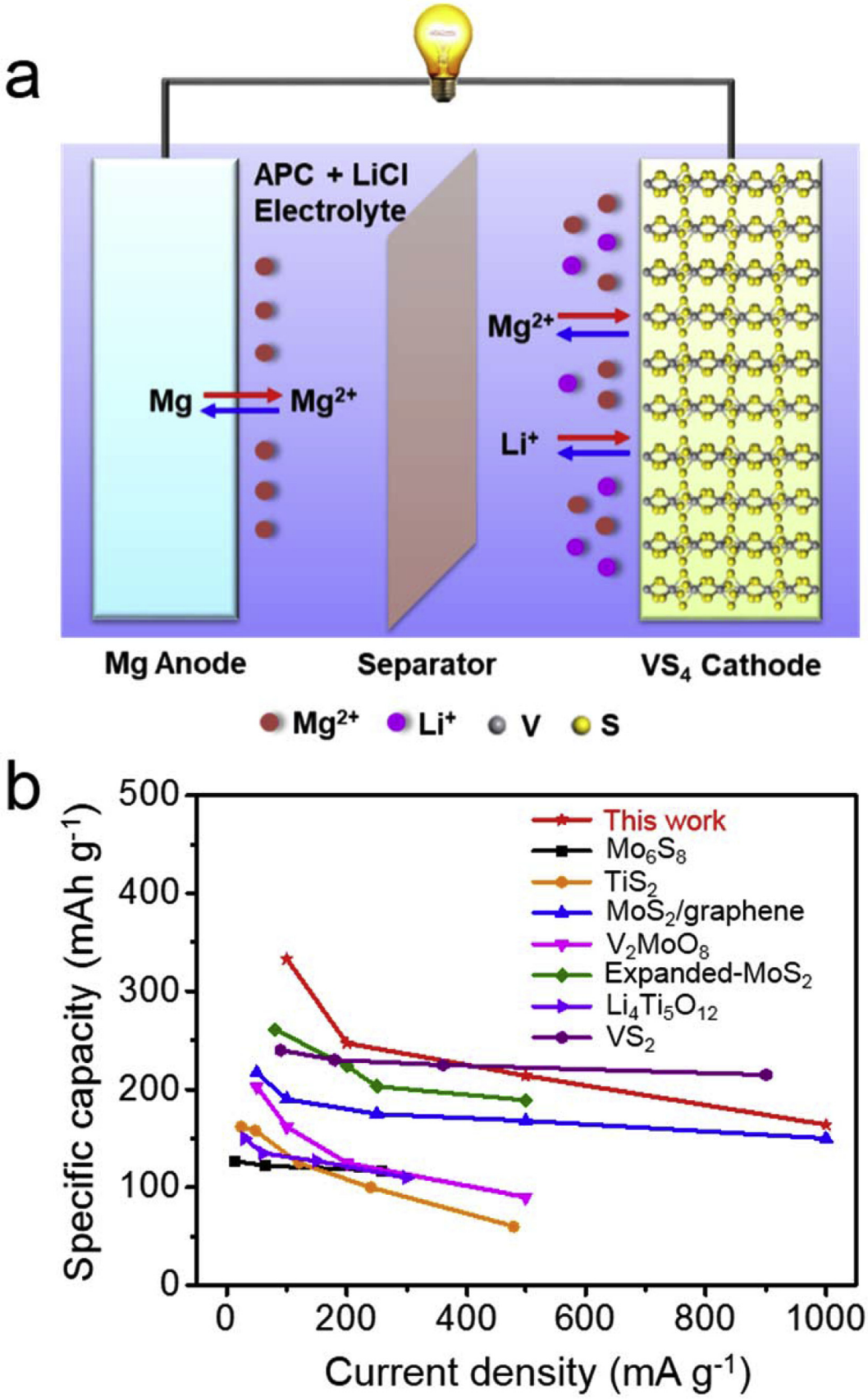

Fig. 6. (a) Schematic illustration of the working mechanism of MLIBs based on VS_4 nanodendrites cathodes. (b) Rate capability plots of MLIBs based on VS_4 nanodendrites cathodes in this work compared with other electrode materials reported in previous literatures [14,19,20,22,35,46,47].

an obvious change in peak intensity (Fig. 5f). The Raman peaks become weaker and broader during the discharge process (from state *1* to state *3*), owing to the Mg^{2+} and Li^{+} insertion into VS_4. Then, the peak intensities gradually recover again during the following charge process (from state *3* to state *5*), which is owing to the extraction of partial Mg^{2+} and Li^{+} ions, in consistence with above XRD results.

The HRTEM images of both discharged and charged VS_4 cathodes in MLIBs are shown in Fig. 5g and h. The HRTEM image (Fig. 5g) of discharged sample displays more obscure lattices, due to the intercalation of Mg^{2+} and Li^{+} ions. The HRTEM image of charged VS_4 nanodendrites (Fig. 5h) show a lattice spacing of 0.56 nm, which is identical to the pristine sample, indicating that the insertion/extraction of Mg^{2+} and Li^{+} ions have little influence to the lattice parameters.

The *ex-situ* XPS, *ex-situ* XRD and *ex-situ* Raman spectra of discharged and charged VS_4 nanodendrites cathode after 20 cycles were also examined (Fig. S5), The morphology of the VS_4 nanodendrites in MLIBs showed a little change after 20 cycles. The corresponding changes of atomic ratios (V^{4+}:V^{5+} and S_2^{2-}:S^{2-}) after 20 cycles are shown in Table S2. The valence states of V and S elements, the Mg^{2+} ion contents and the Raman peak intensities after 20 cycles display similar trends to the 1st cycle, indicating the good reversibility and reproducibility. The intensity of Li 1s band observed from XPS analysis after 20 cycles is weak, which may be due to the fact that Mg^{2+} ions play a leading role in the discharge/charge processes. Moreover, the (110) and (020) peak intensities in the *ex-situ* XRD spectrum after 20 cycles are also weak, possibly because of the reduced crystalline domains and the insertion of Mg^{2+} and Li^{+} ions.

According to the above detailed characterizations, it can be confirmed that both Mg^{2+} and Li^{+} can insert into the VS_4 nanodendrites cathode in MLIBs. The work mechanism of VS_4 nanodendrites cathodes in MLIBs is schematically illustrated in Fig. 6a. The capacity is mainly contributed by Mg^{2+} ions; while Li^{+} ions exhibit lesser contribution to the capacity but very important contribution to the reaction kinetics. Through the insertion of Mg^{2+} and Li^{+} ions into VS_4, $Mg_xLi_yVS_4$ is formed during the discharge steps, leading to the partial reduction of S_2^{2-} to S^{2-} and the partial oxidation of V^{4+} to V^{5+}. During the charge steps, the partial extraction of Mg^{2+} and Li^{+} ions from $Mg_xLi_yVS_4$ makes the valence states of most V^{5+} and S^{2-} change back to V^{4+} and S_2^{2-}. According to the elemental composition variations measured by XPS (Fig. 3a–c), ICP-OES (Table S1) and EDX analysis (Fig. S3), the electrochemical redox processes in the MLIBs can be approximately represented as below:

$$\text{Cathode: } VS_4 + 0.77\,Mg^{2+} + 0.2\,Li^{+} + 1.75\,e^{-} \rightarrow Mg_{0.77}\,Li_{0.21}VS_4 \quad (1)$$

$$Mg_{0.77}\,Li_{0.21}\,VS_4 + 0.63\,Mg^{2+} + 0.49Li^{+} + 1.75e^{-} \leftrightarrow Mg_{1.40}Li_{0.70}VS_4 \quad (2)$$

$$\text{Anode: } Mg \leftrightarrow Mg^{2+} + 2e^{-} \quad (3)$$

The rate capability of VS_4 nanodendrites compared with other hybrid MLIBs reported in literatures are shown in Fig. 6b [14,19,20,22,35,46,47]. In our study, the structure integrity of VS_4 are well preserved, which ensures a superior reversibility and cycle stability of VS_4 in hybrid MLIBs with high capacity retention at 1000 mA g^{-1} after 1500 cycles. Such an impressive electrochemical performance is due to the unique atomic-chain structure of VS_4. The linear open channels in VS_4 are beneficial to the Mg^{2+} and Li^{+} diffusion/migration, and the S_2^{2-} dimers can provide abundant active sites for the storage of Mg^{2+} and Li^{+} ions. Systematic experiments and structural characterizations confirm that both Mg^{2+} and Li^{+} ions are inserted into the open channels of VS_4 1D atomic chains during the discharge-charge processes. Moreover, it could be concluded that the Li^{+} co-insertion is beneficial to create more diffusion pathways and binding sites for Mg^{2+} ion storage and can facilitate ion/charge transfer. Therefore, compared to MIBs, the reversible capacity, rate performance and cycling stability of MLIBs are greatly improved. We hope this study may provide new insights for the design of novel electrode materials for high-performance MLIBs.

Acknowledgements

This work was supported by National Key R&D Program of China (2017YFA0208200, 2016YFB0700600, 2015CB659300), Projects of NSFC (21872069, 51761135104, 21573108), Natural Science Foundation of Jiangsu Province (BK20180008), High-Level Entrepreneurial and Innovative Talents Program of Jiangsu Province, and the Fundamental Research Funds for the Central Universities of China.

Appendix A. Supplementary data

Supplementary data to this article can be found online at https://doi.org/10.1016/j.ensm.2019.06.001.

References

[1] J. Muldoon, C.B. Bucur, A.G. Oliver, T. Sugimoto, M. Matsui, H.S. Kim, G.D. Allred, J. Zajicek, Y. Kotani, Electrolyte roadblocks to a magnesium rechargeable battery, Energy Environ. Sci. 5 (2012) 5941–5950.
[2] D. Aurbach, Z. Lu, A. Schechter, Y. Gofer, H. Gizbar, R. Turgeman, Y. Cohen, M. Moshkovich, E. Levi, Prototype systems for rechargeable magnesium batteries, Nature 407 (2000) 724–727.
[3] J. Muldoon, C.B. Bucur, T. Gregory, Quest for nonaqueous multivalent secondary batteries: magnesium and beyond, Chem. Rev. 114 (2014) 11683–11720.
[4] Y.L. Liang, R.J. Feng, S.Q. Yang, H. Ma, J. Liang, J. Chen, Rechargeable Mg batteries with graphene-like MoS_2 cathode and ultrasmall mg nanoparticle anode, Adv. Mater. 23 (2011) 640–643.
[5] H.D. Yoo, I. Shterenberg, Y. Gofer, G. Gershinsky, N. Pour, D. Aurbach, Mg rechargeable batteries: an on-going challenge, Energy Environ. Sci. 6 (2013) 2265.
[6] Q.D. Truong, M. Kempaiah Devaraju, D.N. Nguyen, Y. Gambe, K. Nayuki, Y. Sasaki, P.D. Tran, I. Honma, Disulfide-bridged (Mo_3S_{11}) cluster polymer: molecular dynamics and application as electrode material for a rechargeable magnesium battery, Nano Lett. 16 (2016) 5829–5835.
[7] E. Levi, Y. Gofer, D. Aurbach, On the way to rechargeable mg batteries: the challenge of new cathode materials, Chem. Mater. 22 (2010) 860–868.
[8] X.Q. Sun, P. Bonnick, V. Duffort, M. Liu, Z.Q. Rong, K.A. Persson, G. Ceder, L.F. Nazar, A high capacity thiospinel cathode for Mg batteries, Energy Environ. Sci. 9 (2016) 2273–2277.
[9] X.Q. Sun, P. Bonnick, L.F. Nazar, Layered TiS_2 positive electrode for Mg batteries, ACS Energy Lett. 1 (2016) 297–301.
[10] Y.W. Cheng, Y.Y. Shao, V. Raju, X.L. Ji, B.L. Mehdi, K.S. Han, M.H. Engelhard, G.S. Li, N.D. Browning, K.T. Mueller, J. Liu, Molecular storage of mg ions with vanadium oxide nanoclusters, Adv. Funct. Mater. 26 (2016) 3446–3453.
[11] K.W. Nam, S. Kim, S. Lee, M. Salama, I. Shterenberg, Y. Gofer, J.S. Kim, E. Yang, C.S. Park, J.S. Kim, S.S. Lee, W.S. Chang, S.G. Doo, Y.N. Jo, Y. Jung, D. Aurbach, J.W. Choi, The high performance of crystal water containing manganese birnessite cathodes for magnesium batteries, Nano Lett. 15 (2015) 4071–4079.
[12] J. Song, M. Noked, E. Gillette, J. Duay, G. Rubloff, S.B. Lee, Activation of a MnO_2 cathode by water-stimulated Mg^{2+} insertion for a magnesium ion battery, Phys. Chem. Chem. Phys. 17 (2015) 5256–5264.
[13] H.S. Kim, T.S. Arthur, G.D. Allred, J. Zajicek, J.G. Newman, A.E. Rodnyansky, A.G. Oliver, W.C. Boggess, J. Muldoon, Structure and compatibility of a magnesium electrolyte with a sulphur cathode, Nat. Commun. 2 (2011) 427.
[14] Y.W. Cheng, Y.Y. Shao, J.G. Zhang, V.L. Sprenkle, J. Liu, G.S. Li, High performance batteries based on hybrid magnesium and lithium chemistry, Chem. Commun. 50 (2014) 9644–9646.
[15] Y.W. Cheng, H.J. Chang, H. Dong, D. Choi, V.L. Sprenkle, J. Liu, Y. Yao, G.S. Li, Rechargeable Mg-Li hybrid batteries: status and challenges, J. Mater. Res. 31 (2016) 3125–3141.
[16] S. Yagi, T. Ichitsubo, Y. Shirai, S. Yanai, T. Doi, K. Murase, E. Matsubara, A concept of dual-salt polyvalent-metal storage battery, J. Mater. Chem. A 2 (2014) 1144–1149.
[17] H.D. Yoo, Y. Liang, Y. Li, Y. Yao, High areal capacity hybrid magnesium-lithium-ion battery with 99.9% coulombic efficiency for large-scale energy storage, ACS Appl. Mater. Interfaces 7 (2015) 7001–7007.
[18] J.H. Cho, M. Aykol, S. Kim, J.H. Ha, C. Wolverton, K.Y. Chung, K.B. Kim, B.W. Cho, Controlling the intercalation chemistry to design high-performance dual-salt hybrid rechargeable batteries, J. Am. Chem. Soc. 136 (2014) 16116–16119.
[19] X. Fan, R.R. Gaddam, N.A. Kumar, X.S. Zhao, A hybrid Mg^{2+}/Li^{+} battery based on interlayer-expanded MoS_2/graphene cathode, Adv. Energy Mater. 7 (2017) 1700317–1700326.
[20] T. Gao, F.D. Han, Y.J. Zhu, L.M. Suo, C. Luo, K. Xu, C.S. Wang, Hybrid Mg^{2+}/Li^{+} battery with long cycle life and high rate capability, Adv. Energy Mater. 5 (2015) 1401507.
[21] S. Su, Y. NuLi, Z. Huang, Q. Miao, J. Yang, J. Wang, A high-performance rechargeable Mg^{2+}/Li^{+} hybrid battery using one-dimensional mesoporous TiO_2 (B) nanoflakes as the cathode, ACS Appl. Mater. Interfaces 8 (2016) 7111–7117.
[22] N. Wu, Z.-Z. Yang, H.-R. Yao, Y.-X. Yin, L. Gu, Y.-G. Guo, Improving the electrochemical performance of the $Li_4Ti_5O_{12}$ electrode in a rechargeable

magnesium battery by lithium-magnesium co-intercalation, Angew. Chem. Int. Ed. 54 (2015) 5757–5761.
[23] Y. Zhang, J.J. Xie, Y.L. Han, C.L. Li, Dual-salt Mg-based batteries with conversion cathodes, Adv. Funct. Mater. 25 (2015) 7300–7308.
[24] S. Britto, M. Leskes, X. Hua, C.A. Hebert, H.S. Shin, S. Clarke, O. Borkiewicz, K.W. Chapman, R. Seshadri, J. Cho, C.P. Grey, Multiple redox modes in the reversible lithiation of high-capacity, peierls-distorted vanadium sulfide, J. Am. Chem. Soc. 137 (2015) 8499–8508.
[25] M.H. Whangbo, P. Gressier, Band-structure of $NbTe_4$, Inorg. Chem. 23 (1984) 1228–1232.
[26] C.S. Rout, B.H. Kim, X. Xu, J. Yang, H.Y. Jeong, D. Odkhuu, N. Park, J. Cho, H.S. Shin, Synthesis and characterization of patronite form of vanadium sulfide on graphitic layer, J. Am. Chem. Soc. 135 (2013) 8720–8725.
[27] X. Xu, S. Jeong, C.S. Rout, P. Oh, M. Ko, H. Kim, M.G. Kim, R. Cao, H.S. Shin, J. Cho, Lithium reaction mechanism and high rate capability of VS_4-graphene nanocomposite as an anode material for lithium batteries, J. Mater. Chem. A 2 (2014) 10847–10853.
[28] Y.L. Zhou, Y.L. Li, J. Yang, J. Tian, H.Y. Xu, J. Yang, W.L. Fan, Conductive polymer-coated VS_4 submicrospheres as advanced electrode materials in lithium-ion batteries, ACS Appl. Mater. Interfaces 8 (2016) 18797–18805.
[29] R.M. Sun, Q.L. Wei, Q.D. Li, W. Luo, Q.Y. An, J.Z. Sheng, D. Wang, W. Chen, L.Q. Mai, Vanadium sulfide on reduced graphene oxide layer as a promising anode for sodium ion battery, ACS Appl. Mater. Interfaces 7 (2015) 20902–20908.
[30] Y.R. Wang, Z.T. Liu, C.X. Wang, X. Yi, R.P. Chen, L.B. Ma, Y. Hu, G.Y. Zhu, T. Chen, Z.X. Tie, J. Ma, J. Liu, Z. Jin, Highly branched VS_4 nanodendrites with 1d atomic-chain structure as a promising cathode material for long-cycling magnesium batteries, Adv. Mater. 30 (2018) 1802563.
[31] G. Silversmit, D. Depla, H. Poelman, G.B. Marin, R. De Gryse, Determination of the V2p xps binding energies for different vanadium oxidation states (V^{5+} to V^{0+}), J. Electron. Spectrosc. Relat. Phenom. 135 (2004) 167–175.
[32] T. Koketsu, J.W. Ma, B.J. Morgan, M. Body, C. Legein, W. Dachraoui, M. Giannini, A. Demortière, M. Salanne, F. Dardoize, H. Groult, O.J. Borkiewicz, K.W. Chapman, P. Strasser, D. Dambournet, Reversible magnesium and aluminium ions insertion in cation-deficient anatase TiO_2, Nat. Mater. 16 (2017) 1142–1148.
[33] H.D. Yoo, Y.L. Liang, H. Dong, J.H. Lin, H. Wang, Y.S. Liu, L. Ma, T.P. Wu, Y.F. Li, Q. Ru, Y. Jing, Q.Y. An, W. Zhou, J.H. Guo, J. Lu, S.T. Pantelides, X.F. Qian, Y. Yao, Fast kinetics of magnesium monochloride cations in interlayer-expanded titanium disulfide for magnesium rechargeable batteries, Nat. Commun. 8 (2017) 339–348.
[34] Y.R. Wang, X.L. Xue, P.Y. Liu, C.X. Wang, X. Yi, Y. Hu, L.M. Ma, G.Y. Zhu, R.P. Chen, T. Chen, J. Ma, J. Liu, Z. Jin, Atomic substitution enabled synthesis of vacancy-rich two-dimensional black TiO_{2-x} nanoflakes for high-performance rechargeable magnesium batteries, ACS Nano 12 (2018) 12492–12502.
[35] X.W. Miao, Z.Y. Chen, N. Wang, Y.N. Nuli, J.L. Wang, J. Yang, S. Hirano, Electrospun V_2MoO_8 as a cathode material for rechargeable batteries with Mg metal anode, Nano Energy 34 (2017) 26–35.
[36] C.B. Bucur, T. Gregory, A.G. Oliver, J. Muldoon, Confession of a magnesium battery, J. Phys. Chem. Lett. 6 (2015) 3578–3591.
[37] D. Aurbach, Y. Gofer, A. Schechter, O. Chusid, H. Gizbar, Y. Cohen, M. Moshkovich, R. Turgeman, A comparison between the electrochemical behavior of reversible magnesium and lithium electrodes, J. Power Sources 97–98 (2001) 269–273.
[38] V. Augustyn, P. Simon, B. Dunn, Pseudocapacitive oxide materials for high-rate electrochemical energy storage, Energy Environ. Sci. 7 (2014) 1597–1614.
[39] Y.L. Zhou, J. Tian, H.Y. Xu, J. Yang, Y.T. Qian, Pseudocapacitive oxide materials for high-rate electrochemical energy storage, Energy Storage Mater. 6 (2017) 149–156.
[40] T. Gao, M. Noked, A.J. Pearse, E. Gillette, X.L. Fan, Y.J. Zhu, C. Luo, L.M. Suo, M.A. Schroeder, K. Xu, S.B. Lee, G.W. Rubloff, C.S. Wang, Enhancing the reversibility of Mg/S battery chemistry through Li^+ mediation, J. Am. Chem. Soc. 137 (2015) 12388–12393.
[41] T. Gao, X. Ji, S. Hou, X. Fan, X. Li, C. Yang, F. Han, F. Wang, J. Jiang, K. Xu, C. Wang, Thermodynamics and kinetics of sulfur cathode during discharge in $MgTFSI_2$-DME electrolyte, Adv. Mater. 30 (2018) 1704313.
[42] X.J. Zhou, J. Tian, J.L. Hu, C.L. Li, High rate magnesium-sulfur battery with improved cyclability based on metal-organic framework derivative carbon host, Adv. Mater. 30 (2018) 1704166.
[43] S.Y. Lang, Y. Shi, Y.G. Guo, R. Wen, L.J. Wan, High-temperature formation of a functional film at the cathode/electrolyte interface in lithium-sulfur batteries: an in situ afm study, Angew. Chem. Int. Ed. 56 (2017) 14433–14437.
[44] M.N. Kozlova, Y.V. Mironov, E.D. Grayfer, A.I. Smolentsev, V.I. Zaikovskii, N.A. Nebogatikova, T.Y. Podlipskaya, V.E. Fedorov, Synthesis, crystal structure, and colloidal dispersions of vanadium tetrasulfide (VS_4), Chem. Eur J. 21 (2015) 4639–4645.
[45] M.S. Weimer, R.F. McCarthy, J.D. Emery, M.J. Bedzyk, F.G. Sen, A. Kinaci, M.K.Y. Chan, A.S. Hock, A.B.F. Martinson, Template-free vapor-phase growth of patronite by atomic layer deposition, Chem. Mater. 29 (2017) 2864–2873.
[46] C.J. Hsu, C.Y. Chou, C.H. Yang, T.C. Lee, J.K. Chang, MoS_2/graphene cathodes for reversibly storing Mg^{2+} and Mg^{2+}/Li^+ in rechargeable magnesium-anode batteries, Chem. Commun. 52 (2016) 1701–1704.
[47] R.M. Sun, C.Y. Pei, J.Z. Sheng, D.D. Wang, L. Wu, S.J. Liu, Q.Y. An, L.Q. Mai, High-rate and long-life VS_2 cathodes for hybrid magnesium-based battery, Energy Storage Mater. 12 (2018) 61–68.